CHEMISTRY
AN ASIAN JOURNAL

DOI: 10.1002/asia.201200045

Sodium 1-Naphthalenesulfonate-Functionalized Reduced Graphene Oxide Stabilizes Silver Nanoparticles with Lower Cytotoxicity and Long-Term Antibacterial Activity

Xiang Cai,[a] Shaozao Tan,*[a] Aili Yu,[a] Jinglin Zhang,[a] Jiahao Liu,[a] Wenjie Mai,[b] and Zhenyou Jiang[c]

Abstract: Silver nanoparticles (AgNPs) are increasingly used in daily life for their antibacterial properties, but their low stability and high cytotoxicity hamper practical applications. In this work, sodium 1-naphthalenesulfonate-functionalized reduced graphene oxide (NA-rGO) was used as a substrate for AgNPs to produce a AgNP-NA-rGO hybrid. This hybrid showed substantially higher antibacterial activity than polyvinyl pyrrolidone(PVP)-stabilized AgNPs, and the AgNPs on NA-rGO were more stable than the AgNPs on PVP, resulting in long-term antibacterial effects. More importantly, this hybrid showed excellent water solubility and low cytotoxicity, suggesting the great potential application as sprayable reduced graphene oxide based antibacterial solutions.

Keywords: antibacterial properties · cytotoxicity · reduced graphene oxide · nanoparticles · silver

Introduction

In order to effectively resolve the microbial pollution and contamination, natural and synthetic antibacterial materials are widely used in daily life. Among them, silver nanoparticles (AgNPs) are well known to be antiseptic to a spectrum of bacteria and are increasingly used for their antibacterial properties in detergents, plastics, food storage containers, antiseptic sprays, catheters, bandages, and textiles.[1] There is a general agreement that the biological action of AgNPs, especially pronounced against microorganisms, is derived from the dissolved silver cation (Ag^+) and its soluble complexes.[2] The function of AgNPs in these ion-based toxicity pathways is 1) to generate a sustained flux of Ag^+ from an inventory of AgNPs bound on substrates or imbedded in matrices or 2) to transport active Ag^+ to sensitive biological targets on cell membranes or within cells following particle attachment or endocytosis, respectively.[3] On the other hand, AgNPs and released Ag^+ have shown cytotoxicity.[4] Some studies showed that AgNPs were more toxic than Ag^+,[5] while others showed the opposite conclusion.[6] Although results from recent studies appear ambiguous, both AgNPs and released Ag^+ shows serious cytotoxicity.[4–6] Moreover, practical applications of AgNPs are often hampered by the aggregation and loss of antibacterial activity.[7] As these facts directly determine the application of AgNPs, and also for assessment of the toxicity of AgNPs in humans, it is highly important to control the release of Ag^+ from AgNPs and to increase the stability of AgNPs. To address this problem, organic[8] and inorganic[9] substances have been employed to stabilize AgNPs or to control the release of Ag^+, and these strategies can partly enhance the antibacterial activity and stability of AgNPs.

To address this challenge, we report herein the first the synthesis of a water-soluble AgNP/sodium 1-naphthalenesulfonate-functionalized reduced graphene oxide (AgNP-NA-rGO) hybrid and demonstrate the excellent stability, long-term antibacterial effect, and lower cytotoxicity of this novel hybrid. The specific benefits of this novel hybrid include 1) dose control to achieve desired antibacterial effects; 2) dose limitation to avoid eukaryotic toxicity; 3) control of product lifetime before dissolution and diffusion end antibacterial activity; 4) sprayable antibacterial solutions.

Results and Discussion

Formation Mechanism and Water Solubility of AgNP-NA-rGO

The AgNP-NA-rGO hybrid was prepared by a three-step approach as illustrated in Scheme 1. Under the present experimental conditions, only graphene oxide (GO) is suitable

[a] Dr. X. Cai, Prof. S. Tan, A. Yu, J. Zhang, J. Liu
Department of Chemistry, Jinan University
Guangzhou 510632 (P. R. China)
Fax: (+86) 20-8522-3670
E-mail: shaozao@tom.com

[b] Prof. W. Mai
Department of Physics, Jinan University
Guangzhou 510632 (P. R. China)

[c] Prof. Z. Jiang
Department of Microbiology and Immunology
Medical School of Jinan University
Guangzhou 510632 (P. R.China)

Supporting information for this article is available on the WWW under http://dx.doi.org/10.1002/asia.201200045.

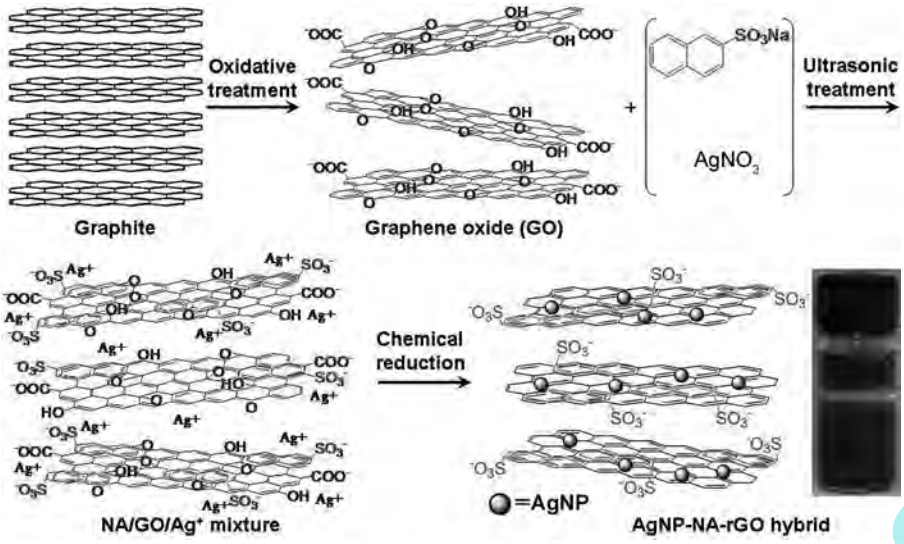

Scheme 1. The synthesis of water-soluble AgNP-NA-rGO hybrid. Step 1) oxidative treatment of graphite yields single-layer GO. Step 2) The ultrasonic treatment of GO in the presence of sodium 1-naphthalenesulfonate (NA) and silver nitrate produces a NA/GO/Ag^+ mixture. Step 3) The chemical reduction of GO and Ag^+ with hydrazine monohydrate produces a water-soluble AgNP-NA-rGO dispersion.

for the preparation of AgNP-NA-rGO hybrid. The nucleation of AgNPs at GO surfaces should be mainly governed by the presence of oxygen groups at GO and sulfate groups at NA, which contribute to an overall negatively charged surface, and the overall negatively charged functional groups are responsible for the previous attachment of the free Ag^+ in solution because of electrostatic interactions. Afterward, the addition of the reducing agent to the precursor solution promotes the subsequent reduction of GO and Ag^+, enabling the growth of AgNPs at the graphene surface.[10] The dark blue, homogeneous dispersion (Scheme 1) with concentration up to 1.1 mg mL^{-1} was found to remain stable without visible precipitation for more than three months.

The thickness of the NA-functionalized reduced graphene oxide (NA-rGO) is approximately 0.6 nm, as determined by AFM (Figure 1 A), which is greater than that of single-layer graphene (0.334 nm). The increase in thickness may be attributed to the absorption of NA on the reduced graphene oxide (rGO) surface, and the NA could assemble on surfaces of rGO through π–π interactions.

To examine this hypothesis, fluorescence spectra of NA (1.6 mg L^{-1}) upon gradual addition of rGO (0–2.0 mg L^{-1}) in aqueous solution were recorded. As shown in Figure 2, the significant quenching of the NA fluorescence by rGO was caused by effective photoinduced charge transfer between these components,[11] which demonstrated that the NA was noncovalently adhered to the surface of rGO, and the π stacking of NA greatly enhanced the aqueous solubility of AgNP-NA-rGO.

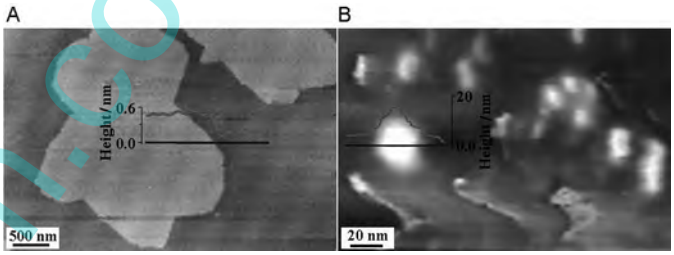

Figure 1. A) Tapping-mode AFM image of NA-rGO on a clean mica surface and cross-sectional profile of NA-rGO. B) Tapping-mode AFM image of AgNP-NA-rGO on a clean mica surface and cross-sectional profile of AgNPs.

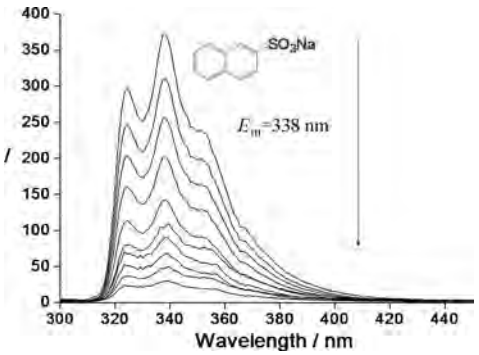

Figure 2. Fluorescence spectra of NA (1.6 mg L^{-1}) upon gradual addition of rGO in aqueous solution (0–2.0 mg L^{-1} in increments of 0.2 mg L^{-1} from top to bottom) with an excitation wavelength of 273 nm (25 °C).

The dispersion of the AgNPs on the 2D sheet of NA-rGO can be visualized in the AFM image in Figure 1 B and the

Abstract in Chinese:

由于具有抗菌性能，纳米银已经越来越广泛地用于日常生活中，但是，纳米银的毒性和低的稳定性限制了它的应用范围。在本工作中，萘磺酸钠功能化还原氧化石墨被用作纳米银的基材，制备了萘磺酸钠-还原氧化石墨-纳米银复合物。所制备的复合物具有比聚乙烯吡咯烷酮稳定的纳米银更强的抗菌活性，而且纳米银在萘磺酸钠功能化还原氧化石墨基材上的稳定性高于聚乙烯吡咯烷酮稳定的纳米银，从而使得萘磺酸钠-还原氧化石墨-纳米银复合物具有更长效的抗菌活性。更重要的是，萘磺酸钠-还原氧化石墨-纳米银复合物具有良好的水溶性和更低的毒性，预示着其可以作为一种基于还原氧化石墨的可喷洒的抗菌溶液。

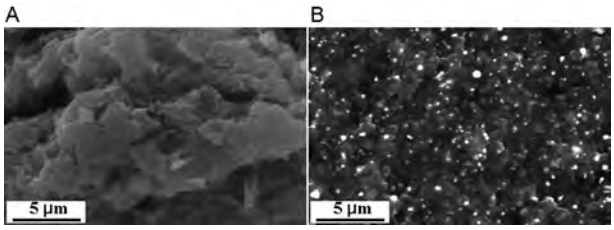

Figure 3. SEM images of A) NA-rGO and B) AgNP-NA-rGO.

SEM image in Figure 3. The SEM analysis confirms the ability to attain 3–20 nm diameter AgNPs anchored on the NA-rGO nanosheets. The corrugated nature of the NA-rGO sheets is evident by AFM analysis (Figure 1B).

The TEM micrograph in Figure 4A further depicts a representative image of AgNP-NA-rGO. The thin structure of

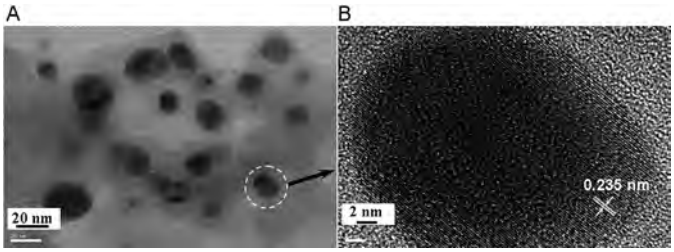

Figure 4. A) TEM image of AgNP-NA-rGO, B) HRTEM image of AgNPs with fringe spacing.

the AgNP-NA-rGO and porous surface are confirmed. Analysis of the image shows the distribution of AgNPs on the surface of the NA-rGO with particle sizes roughly in the range of 3–20 nm. The measured fringe lattice of an exemplary AgNP (Figure 4B) is found to be 0.235 nm, which corresponds to the (111) crystal plane of the AgNP. Figure 5

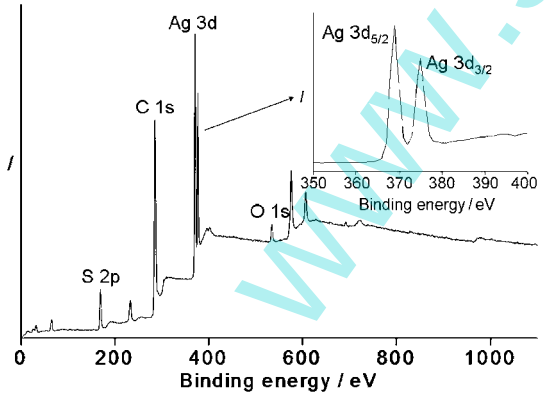

Figure 5. XPS profiles of AgNP-NA-rGO.

shows the X-ray photoelectron spectroscopy (XPS) analysis of AgNP-NA-rGO. The binding energies of 368.8 and 374.8 eV were attributed to Ag $3d_{5/2}$ and Ag $3d_{3/2}$, respectively. The 6.0 eV splitting of the 3d doublet of silver indicated the formation of AgNPs on the surface of NA-rGO.[12]

These results indicated that AgNPs were formed on the NA-rGO. What is more, the binding energy of 168.1 eV was attributed to S 2p of NA, which corresponded to the sulfur atom in the sulfate groups of NA of AgNP-NA-rGO. These results were further confirmed by XRD patterns in Figure S1 in the Supporting Information.

Then, the excellent water solubility of the AgNP-NA-rGO hybrid was displayed. The AgNP-NA-rGO dispersion showed a Tyndall effect (Scheme 1), and a negative zeta potential of −42.3 mV was found for AgNP-NA-rGO in aqueous solution at a concentration around 0.10 mg mL^{-1} (pH 7, prepared by diluting the purified AgNP-NA-rGO in ultrapure water). According to the definition of colloid stability with zeta potential by the ASTM (American Society for Testing and Materials) standard D4187-82,[13] the AgNP-NA-rGO dispersion in the aqueous solution has ''good stability'' with zeta potential values between ±40 and ±60 mV. Inductively coupled plasma (ICP) analysis provided quantitative evidence for the presence of 3.6 mg Ag L^{-1} in 0.10 mg mL^{-1} AgNP-NA-rGO dispersion, which means the AgNP content in AgNP-NA-rGO is 3.6 wt%.

Release Properties and Stability of AgNP-NA-rGO

According to the previous experimental results, it can be safely assumed that the detected amounts of silver from dialysis experiments are due to only Ag^+ and not to AgNPs.[2] For AgNP-NA-rGO and poly(vinyl pyrrolidone) AgNPs (PVP-AgNPs), the diffusion of Ag^+ out of the dialysis tube was slow; after five days, only 32.1% and 66.8% Ag^+ were removed by dialysis, respectively (Figure 6). As the AgNP-

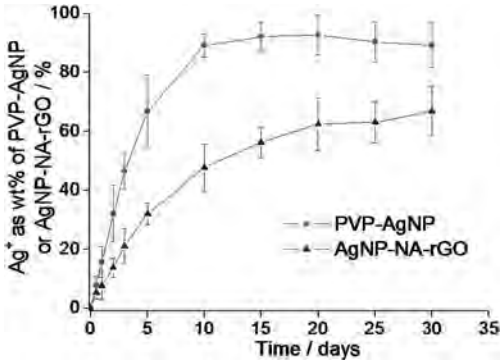

Figure 6. Dissolution data collected from PVP-AgNPs and AgNP-NA-rGO at 35°C.

NA-rGO shows lower release speed than PVP-AgNPs, the AgNP-NA-rGO should display a longer-term antibacterial effect than PVP-AgNPs. The majority of Ag^+ comes from oxidation of the zero-valent AgNPs, typically by reaction with dissolved O_2 and mediated by protons and other components in the surrounding fluid phase [Equations (1) and (2)].[14]

$$AgNP + O_2 \rightarrow AgNP \cdots O_2 \xrightarrow{H^+} Ag^+ + \text{reactive oxygen intermediates} \quad (1)$$

$$\text{Reactive oxygen intermediates} + AgNP \xrightarrow{H^+} Ag^+ + H_2O \quad (2)$$

Methods that disrupt oxidation pathways are promising routes to slow the release of Ag^+ from AgNP surfaces. Many AgNP formulations use macromolecular coatings such as dextran,[8b] starch,[8c] gum arabic,[8d] or synthetic polymers,[8e] which can block oxygen access.[8f] We observe here that NA and rGO can more efficiently delay and extend Ag^+ release from AgNPs than PVP. On the one hand, rGO made two contributions to delay and extend Ag^+ release. First, the oxidation process makes rGO retain many holes (shown in Figure 7); since the O_2 chemisorption on rGO

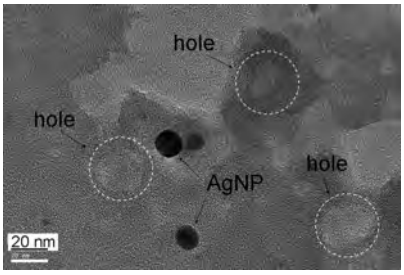

Figure 7. The microstructure of AgNP-NA-rGO.

edges is exothermic,[15] and the O_2 adsorption on AgNPs is endothermic,[16] the rGO can adsorb some of the oxygen that would otherwise have access to AgNPs. Second, rGO still contains a large number of active groups (hydroxy, aldehyde, and epoxy groups); these active groups can scavenge reactive oxygen intermediates from the surrounding medium. On the other hand, the negatively charged sulfate groups of NA can attract protons from the surrounding medium and interfere with the oxidation reaction, thus slowing the release of Ag^+ from AgNPs.

PVP-AgNPs are easily aggregated in light, which usually leads to significant reduction of antibacterial activity.[17] Corresponding UV/Vis spectra showed that, upon extended exposure to light, the absorption peak of PVP-AgNPs at 408 nm shifted to 419 nm with a large decrease in intensity, suggesting aggregation of AgNPs (Figure 8 A).[18] In comparison, the UV/Vis spectra of the AgNP-NA-rGO changed little when stored either in dark or light for seven days (Figure 8 B). Therefore, AgNP-NA-rGO is much more stable and resistant to aggregation than PVP-AgNPs. The high stability of AgNPs at the surface of the rGO anchored the AgNPs to the surface and prevented their aggregation. Since the nanoparticle suspensions will be exposed to environmental conditions different from a research lab setting, many factors, including light, temperature, salinity, and so forth, are suspected to affect the stability of the nanoparti-

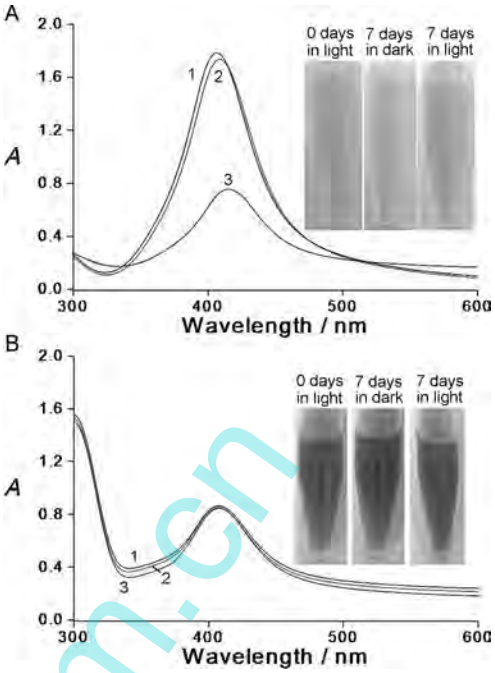

Figure 8. Stability comparison of AgNP-NA-rGO and PVP-AgNPs. The absorption spectra of A) PVP-AgNPs and B) AgNP-NA-rGO with a surface plasmon resonance band: 1) new synthesis, 2) stored in dark, 3) stored in light. Insets: digital photographs of the samples under different conditions.

cle. So, the high stability of AgNP-NA-rGO is very important for the use of the antibacterial material in environmental conditions. Given that the release properties and aggregation states of PVP-AgNPs are critical to antibacterial activity, we conclude that the long-term antibacterial activity and high stability of the AgNP-NA-rGO is responsible for their practical application.

Synergistic Antibacterial Activity of AgNP-NA-rGO

Table 1 shows the antibacterial activity of NA-rGO, PVP-AgNPs, and AgNP-NA-rGO after 6 h contact with bacteria. At low concentration (96.4 mg L^{-1}), NA-rGO showed no an-

Table 1. The antibacterial activity of the newly prepared samples.

Sample	AgNPs [mg L^{-1}]	NA-rGO [mg L^{-1}]	Colonies[a] [cfu mL^{-1}]	Sterilizing rate [%]
		E. coli		
blank sample	0	0	1.81×10^6	–[b]
NA-rGO	0	96.4	1.81×10^6	–[b]
NA-rGO	0	964	$1.67–1.68\times10^6$	7.5 ± 0.4
PVP-AgNPs	3.6	0	$2.03–2.06\times10^5$	88.7 ± 0.1
AgNP-NA-rGO	3.6	96.4	$1.21–1.54\times10^5$	92.4 ± 0.9
		S. aureus		
blank sample	0	0	1.28×10^6	–[b]
NA-rGO	0	96.4	1.28×10^6	–[b]
NA-rGO	0	964	$1.13–1.14\times10^6$	11.2 ± 0.3
PVP-AgNPs	3.6	0	$0.86–1.16\times10^5$	92.1 ± 1.2
AgNP-NA-rGO	3.6	96.4	$3.33–4.61\times10^4$	96.9 ± 0.5

[a] Colonies of bacteria after 6 h contact. [b] No effect.

tibacterial activity, and the viable colonies of *E. coli* or *S. aureus* remained essentially unchanged. When the concentration of NA-rGO reached 964 mg L^{-1}, the sterilizing rate against *E. coli* and *S. aureus* is 7.5% and 11.2%, respectively. It was shown that the antibacterial activity was enhanced when AgNPs were deposited on the NA-rGO surface, but it didn't mean that the antibacterial activity was the simple addition of the antibacterial activity of NA-rGO and AgNPs. However, the AgNP-NA-rGO showed obvious synergistic antibacterial effects. Because graphene is a single-atom-thick two-dimensional graphitic carbon material, this extremely thin nanomaterial possesses extraordinary thermal, mechanical, and electrical properties.[19] Recently, research attention has been drawn towards the antibacterial activity of graphene and its composite materials.[20] In our previous study, we reported a graphene-based antibacterial composite combining the advantages of graphene and an organic antibacterial agent. This system displayed excellent synergistic antibacterial activity, specific-targeting capability, water solubility, and mild cytotoxicity.[20c] We suggest that the "blade-like edges" of AgNP-NA-rGO can damage the cytoplasmic membrane of the bacterial cell,[20c] which will more quickly and conveniently allow the Ag^+ to react with cytoplasmic constituents and eventually kill the bacteria. So, we suggest that the AgNP-NA-rGO combined the advantages of both graphene and Ag^+ on antibacterial activity, thus rendering the Ag^+ more efficient against bacteria, and the use of AgNPs will be more efficient. Furthermore, compared to Gram-positive species (*S. aureus*), the Gram-negative strain (*E. coli*) has an outer membrane outside the peptidoglycan layer,[21] which is composed mainly of lipopolysaccharides and phospholipids. The outer membrane plays a significant role in protecting the bacterial cells from attack by foreign compounds.[21] So, all samples showed lower antibacterial activity towards *E. coli*.

Cytotoxicity of AgNP-NA-rGO

The 3-(4,5-dimethylthiahiazol-2-y1)-3,5-diphenyltetrazolium-bromide (MTT) assays (Figure 9) showed that NA-rGO (25 μg mL^{-1}) exhibited a slight cytotoxicity (ca. 16%) to nasopharyngeal carcinoma cell lines (CNE1) within 24 h incubation. For PVP-AgNPs, the cell viability of CNE1 was reduced to 47% and 31% with PVP-AgNPs at concentrations of 25 and 100 μg mL^{-1}, respectively. However, the cell viability of CNE1 was increased to 57% and 37% with AgNP-NA-rGO at concentrations of 25 and 100 μg mL^{-1}, respectively. Therefore, the cytotoxicity of AgNP-NA-rGO was slightly lower than that of PVP-AgNPs. The result was in accordance with the result of inverted phase contrast microscope measurements (Figure 10). Such difference in cytotoxicity might arise from the different functional groups and the different surface charges of PVP-AgNPs and AgNP-NA-rGO surfaces.[22] Compared with other studies,[22] we concluded that AgNP-NA-rGO were relatively biocompatible nanomaterials with mild cytotoxicity.

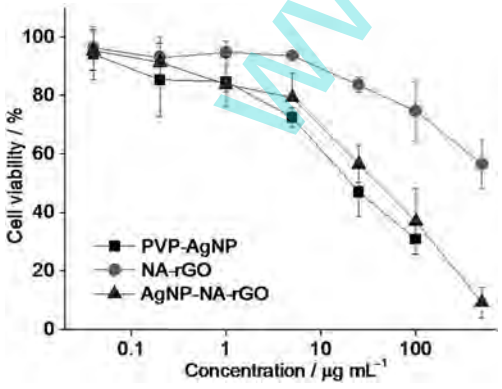

Figure 9. Cytotoxicity of PVP-AgNPs, NA-rGO, and AgNP-NA-rGO on CNE1 cells.

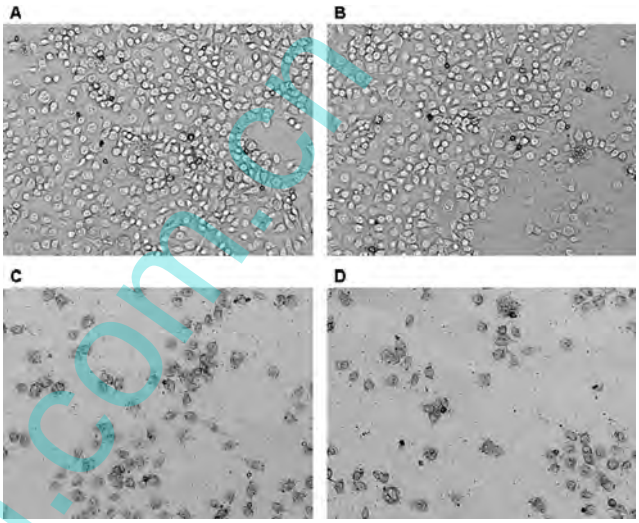

Figure 10. Morphologic changes of CNE1 cells in a control group and experimental groups. A) In the control group, the CNE1 cells had good shape, presented long fusiform or polygon. The presence of round dividing cells showed their vigorous growth. B) The CNE1 cells shape became irregular after 24 h when the concentration of NA-rGO was set at 500 μg mL^{-1}. C) The CNE1 cells shape became more irregular, and the shapes of majority of the cells were injured after 24 h when the concentration of AgNP-NA-rGO was set at 500 μg mL^{-1}. D) The number of CNE1 cells decreased significantly, and the shapes of majority of the cells were seriously injured after 24 h when the concentration of PVP-AgNPs was set at 500 μg mL^{-1}. Pictures are 1.333 mm × 1.000 mm.

Conclusions

In summary, we described a AgNP-NA-rGO hybrid which was prepared by using noncovalent NA-rGO as the carrier of AgNPs. With negative zeta potential of −42.3 mV, the AgNP-NA-rGO dispersion was found to remain stable for more than three months without visible precipitate. The solubility of AgNP-NA-rGO could reach up to 1.1 mg mL^{-1}, and the AgNP content in AgNP-NA-rGO was 3.6 wt%. The

high stability of AgNPs at the surface of the rGO anchored the AgNPs to the surface and prevented their aggregation. The rGO could more efficiently delay and extend Ag^+ release from AgNPs than PVP, and AgNP-NA-rGO showed longer-term antibacterial effects than PVP-AgNPs. The AgNP-NA-rGO hybrid showed obvious synergistic antibacterial effects: the "blade-like edges" of AgNP-NA-rGO could damage the cytoplasmic membrane of the bacterial cell, which would make the Ag^+ react with cytoplasmic constituents more quickly and conveniently and eventually kill the bacteria. The AgNP-NA-rGO was found to be a relatively biocompatible nanomaterial with mild cytotoxicity. Given these advantages, we expect that the AgNP-NA-rGO hybrid is a promising antibacterial material for environmental applications.

Experimental Section

The details for the materials are described in the Supporting Information.

Graphene oxide was prepared by oxidizing natural graphite powder based on a modified Hummers method as originally presented by Kovtyukhova et al.[23] As-prepared GO supernatant (10 mL, 20 mg mL^{-1}) was distributed in ultrapure water (40 mL) to obtain a homogeneous, stable dispersion with the aid of ultrasonication in a water bath (KQ218, 60 W). Then NA (400 mg) and silver nitrate (100 mg) were added to the GO dispersion. After 2 h sonication, hydrazine monohydrate (10 mL, 50 wt% in water) was added under stirring, and the reduction reaction proceeded at 30 °C for 0.5 h. After that, another portion of hydrazine monohydrate (10 mL, 50 wt% in water) was added and the reduction reaction proceeded at 85 °C for 48 h, at which time a homogeneous green-black dispersion was obtained. The resulting solution was then filtered through a polycarbonate membrane (0.22 μm pore size) and repeatedly washed by ultrapure water to remove the excess free NA and silver nitrate. The collected AgNP-NA-rGO hybrid was redistributed in ultrapure water by ultrasonication in a water bath (KQ218, 60 W) for 15 min. NA-rGO was prepared without silver nitrate. PVP-AgNPs was prepared by reducing silver nitrate with glucose in the presence of PVP according to the method of Wang et al.[24]

Zeta potential measurements were performed using a zeta sizer nano ZS (Malvern Instruments), and all the aqueous samples were diluted to 0.05 mg mL^{-1} before measurements. XPS profiles were recorded by an ESCALAB 250 X-ray photoelectron spectrometer (Thermo-VG Scientific). TEM images were observed by using a JEOL JEM-2100F transmission electron microscope. UV/Vis spectra were recorded by a Hitachi 330 UV-Vis spectrophotometer. Raman spectra were obtained with a Renishaw inVia spectrometer, and the 514.5 nm radiation from a 20 mW air-cooled argon ion laser was used as the excitation source. AFM images were observed by an atomic force microscope (AFM, Benyuan CSPM5500) on a flat mica substrate.

For antibacterial tests, the freshly prepared samples were dispensed into sterile 0.8 wt.% saline water (10 mL) containing about 10^6 cfu mL^{-1} *E. coli* ATCC 8099 or *S. aureus* ATCC 6538, and then shaken at 37 °C. After 6 h contact, 0.1 mL of the suspension was taken out from the test tube and diluted to a defined volume (to ensure the bacterial colonies grown could be counted easily and correctly) by ten-fold dilution. The diluted solution was plated on Luria Bertani broth agar plates in triplicate and incubated at 37 ± 1 °C for 24 h. The sterilizing rate (η) is relative to the viable bacteria counts as follows: $\eta = (Y-X) \times 100\%/Y$, where Y is the number of microorganism colonies on the control tube (a sterile 0.8 wt.% saline water without sample) and X is the number of microorganism colonies on the samples. The test was repeated three times.

Release properties of AgNP-NA-rGO were tested by dialysis experiments.[2] Dialysis experiments were carried out in dialysis tubes (Spectra/Por Biotech; cellulose ester; MWCO 100 000) filled with 5 mL solution or dispersion and immersed in 500 mL ultrapure water. The dialysis was carried out under slow stirring with a magnetic stirrer at 35 °C. The concentration of Ag^+ was measured by ICP-MS.

Cytotoxicity of AgNP-NA-rGO was tested using the MTT assay based on the cellular uptake of MTT and its subsequent reduction in the mitochondria of living cells to dark blue MTT formazan crystals.[25] CNE1 cells were seeded on 96-well plates ($1.5–2 \times 10^4$ cells per well) in corresponding medium. Then, the cells were treated with the PVP-AgNPs, NA-rGO, or AgNP-NA-rGO for 24 h. After that, MTT (5 mg mL^{-1} in phosphate-buffered saline) was added to each well and incubated for additional 4 h (37 °C, 5% CO_2). The cells were then lyzed in dimethyl sulfoxide (150 μL per well) and the plates were allowed to stay in the incubator (37 °C, 5% CO_2) to dissolve the purple formazan crystals. The color intensity reflecting cell viability was read at 490 nm using a Model-550 Enzyme-linked immunosorbent microplate (Bio-Rad, USA), and the morphologic changes of CNE1 cells were photographed by a IX-70 inverted phase contrast microscope (Olympus, Japen). All the experiments were repeated four times and Statistical Product and Service Solutions software was used to assess statistical significance of the differences among treatment groups.

Acknowledgements

This work was financially supported by the National Natural Science Foundation of China (51172099, 21006038 and 51102115), the Natural Science Key Foundation of Guangdong Province of China (10251007002000000), and the Fundamental Research Funds for the Central Universities (21610102), the Undergraduate Scientific and Technological Innovation Project of Guangdong Province (1055911018), and the Undergraduate Scientific and Technological Innovation Project of Jinan University (cx11128).

[1] a) T. M. Benn, P. Westerhoff, *Environ. Sci. Technol.* **2008**, *42*, 4133–4139; b) S. A. Blaser, M. Scheringer, M. MacLeod, K. Hungerbuhler, *Sci. Total Environ.* **2008**, *390*, 396–409.
[2] S. Kittler, C. Greulich, J. Diendorf, M. Köller, M. Epple, *Chem. Mater.* **2010**, *22*, 4548–4554.
[3] J. Liu, D. A. Sonshine, S. Shervani, R. H. Hurt, *ACS Nano* **2010**, *4*, 6903–6913.
[4] M. Ahamed, M. S. AlSalhi, M. K. J. Siddiqui, *Clin. Chim. Acta* **2010**, *411*, 1841–1848.
[5] a) C. Greulich, S. Kittler, M. Epple, G. Muhr, M. Köller, *Langenbecks Arch. Surg.* **2009**, *394*, 495–502; b) S. Kittler, C. Greulich, M. Köller, M. Epple, *Materialwiss. Werkstofftech.* **2009**, *40*, 258–264.
[6] P. V. Asharani, Y. L. Wu, Z. Gong, S. Valiyaveettil, *Nanotechnology* **2008**, *19*, 255102.
[7] H. Kong, J. Jang, *Langmuir* **2008**, *24*, 2051.
[8] a) K. H. Wu, C. I. Liu, C. C. Yang, G. P. Wang, C. M. Chao, *Mater. Chem. Phys.* **2011**, *125*, 802–806; b) Y. Ma, J. Yi, L. A. Zhang, *J. Macromol. Sci. Part A* **2009**, *46*, 643–648; c) P. V. Asharani, G. L. K. Mun, M. P. Hande, S. Valiyaveettil, *ACS Nano* **2009**, *3*, 279–290; d) Y. N. Rao, D. Banerjee, A. Datta, S. K. Das, R. Guin, A. Saha, *Radiat. Phys. Chem.* **2010**, *79*, 1240–1246; e) M. Chen, L. Wang, J. Han, J. Zhang, Z. Li, D. Qian, *J. Phys. Chem. B* **2006**, *110*, 11224–11231; f) R. B. Grubbs, *Polym. Rev.* **2007**, *47*, 197–215; g) X. Zan, M. Kozlov, T. J. McCarthy, Z. Su, *Biomacromolecules* **2010**, *11*, 1082–1088.
[9] M. Lv, S. Su, Y. He, Q. Huang, W. Hu, D. Li, C. Fan, S. Lee, *Adv. Mater.* **2010**, *22*, 5463–5467.
[10] G. Goncalves, P. A. A. P. Marques, C. M. Granadeiro, H. I. S. Nogueira, M. K. Singh, J. Grácio, *Chem. Mater.* **2009**, *21*, 4796–4802.
[11] a) X. Qi, K. Y. Pu, X. Zhou, H. Li, B. Liu, F. Boey, W. Huang, H. Zhang, *Small* **2010**, *6*, 663–669; b) Z. Yang, X. Shi, J. Yuan, H. Pu, Y. Liu, *Appl. Surf. Sci.* **2010**, *257*, 138–142.

[12] Y. Liu, X. Wang, F. Yang, X. Yang, *Microporous Mesoporous Mater.* **2008**, *114*, 431–439.
[13] *Zeta Potential of Colloids in Water and Waste Water*, ASTM Standard D4187–82, American Society for Testing and Materials, **1985**.
[14] J. Liu, R. H. Hurt, *Environ. Sci. Technol.* **2010**, *44*, 2169–2175.
[15] S. Klacar, A. Hellman, I. Panas, H. Grönbeck, *J. Phys. Chem. C* **2010**, *114*, 12610–12617.
[16] L. Tsetseris, S. T. Pantelides, *J. Phys. Chem. B* **2009**, *113*, 941–944.
[17] a) A. Henglein, *Chem. Mater.* **1998**, *10*, 444; b) C. N. Lok, C. M. Ho, R. Chen, Q. Y. He, W. Y. Yu, H. Sun, P. K. H. Tam, J. F. Chiu, C. M. Che, *J. Biol. Inorg. Chem.* **2007**, *12*, 527.
[18] a) X. Li, J. Zhang, W. Xu, H. Jia, X. Wang, B. Yang, B. Zhao, B. Li, Y. Ozaki, *Langmuir* **2003**, *19*, 4285; b) Z. Shi, K. G. Neoh, E. T. Kang, *Langmuir* **2004**, *20*, 6847.
[19] a) J. A. Matthew, C. T. Vincent, B. K. Richard, *Chem. Rev.* **2010**, *110*, 132–145; b) D. Chen, L. Tang, J. Li, *Chem. Soc. Rev.* **2010**, *39*, 3157–3180; c) H. Zhang, X. Lv, Y. Li, Y. Wang, J. Li, *ACS Nano* **2010**, *4*, 380–386; d) J. Liu, Y. Li, Y. Li, J. Li, Z. Deng, *J. Mater. Chem.* **2010**, *20*, 900–906; e) Y. Wang, Z. Li, J. Wang, J. Li, Y. Lin, *Trends Biotechnol.* **2011**, *29*, 205–212; f) Y. Wang, Y. Shao, D. W. Matson, J. Li, Y Lin, *ACS Nano* **2010**, *4*, 1790–1798; g) T. Wu, X. Cai, S. Tan, H. Li, J. Liu, W. Yang, *Chem. Eng. J.* **2011**, *173*, 144–149; <lit h>X. Cai, S. Tan, A. Xie, M. Lin, Y. Liu, X. Zhang, Z. Lin, T. Wu, W. Mai, *Mater. Res. Bull.* **2011**, *46*, 2353–2358.
[20] a) J. Shen, M. Shi, N. Li, H. Ma, M. Ye, *Nano Res.* **2010**, *3*, 339; b) W. Hu, C. Peng, W. Luo, M. Lv, X. Li, D. Li, Q. Huang, C. Fan, *ACS Nano* **2010**, *4*, 4317; c) X. Cai, S. Tan, M. Lin, A. Xie, W. Mai, X. Zhang, Z. Lin, T. Wu, Y. Liu, *Langmuir* **2011**, *27*, 7828.
[21] a) Y. H. Yang, G. J. Dai, S. Z. Tan, Y. L. Liu, Q. S. Shi, Y. S. Ouyang, *J. Rare Earth* **2011**, *29*, 308; b) S. Z. Tan, K. H. Zhang, L. L. Zhang, Y. S. Xie, Y. L. Liu, *Chin. J. Chem.* **2008**, *26*, 865.
[22] X. Zhang, Y. Feng, S. Tang, W. Feng, *Carbon* **2010**, *48*, 211–216.
[23] a) W. S. Hummers, R. E. Offeman, *J. Am. Chem. Soc.* **1958**, *80*, 1339–1339; b) N. I. Kovtyukhova, P. J. Ollivier, B. R. Martin, T. E. Mallouk, S. A. Chizhik, E. V. Buzaneva, A. D. Gorchinskiy, *Chem. Mater.* **1999**, *11*, 771–778.
[24] H. Wang, X. Qiao, J. Chen, S Ding, *Colloids Surf. A* **2005**, *256*, 111–115.
[25] M. Ceckova, Z. Vackova, H. Radilova, A. Libra, M. Buncek, F. Staud, *Toxicol. in Vitro* **2008**, *22*, 1846–1852.

Received: January 13, 2012
Published online: March 27, 2012

